A COMPARISON OF TEST METHODS FOR EARLY-AGE BEHAVIOR OF CEMENTITIOUS MATERIALS

J.W. Bullard (1), M. D'Ambrosia (2), Z. Grasley (2), W. Hansen (3), N. Kidner (4), D. Lange (2), P. Lura (5), T.O. Mason (4), J. Moon (6), F. Rajabipour (6), G. Sant (6), S. Shah (4), Z. Sun (4), T. Voigt (4), S. Wansom (4), J. Weiss (6), and L. Woo (4)

(1) NIST, Gaithersburg, Maryland, USA

(2) University of Illinois at Urbana-Champaign, Urbana, Illinois USA

(3) University of Michigan, Ann Arbor, Michigan, USA

(4) Northwestern University, Evanston, Illinois USA

(5) Technical University of Denmark, Lyngby, DENMARK

(6) Purdue University, West Lafayette, Indiana USA

Abstract

A wide range of tests has been reported that can be used for probing different aspects of the chemical and structural properties of cement paste and concrete at early ages. In principle, these tests should be complementary and their results could be integrated to develop a broader understanding of early-age behaviour. Under the auspices of the Center for Advanced Cement Based Materials (ACBM), an inter-laboratory study was undertaken to compare the results of several of these different test methods on a single cement. A large quantity of cement was homogenized by the Cement and Concrete Reference Laboratory (CCRL), as part of their proficiency sample program, and distributed to several ACBM researchers for independent testing. Aggregates for making mortar were supplied from a single source (graded Ottawa sand). Tests on pastes and mortars included calorimetry, compressive strength, Vicat needle penetration, chemical shrinkage, autogenous shrinkage, AC-impedance spectroscopy, time domain reflectometry, and ultrasonic shear wave reflectometry. Numerical simulations of the same materials were undertaken for comparison. Results from these tests will be compared with respect to the way in which they capture solidification and strength development.

1. INTRODUCTION

One of the most interesting and challenging aspects of studying cementitious systems at early ages (up to 7 d) is the large number of time-dependent observations that can be used to characterize the progress of the hydration reactions. Direct measurements of the volume

fractions of each solid phase as a function of time, although ideal, are difficult to obtain under ordinary laboratory conditions. Indirect measurements, which characterize some property that is strongly correlated to the extent of hydration, are much more common. A large number of possibilities exist. Thermogravimetric methods are frequently used to measure the loss on ignition (LOI) of a partially hydrated cement paste. Calorimetric methods, which indicate the sum of the heat released by the collective chemical reactions, are also well established. Nuclear magnetic resonance spectroscopy (NMR) can detect the relative quantities of bound and free water in a paste, thereby providing an indication of the macroscopic degree of hydration. Alternatively, some indirect measures of structural development include measurements of setting time (e.g., by Vicat needle penetration), compressive strength, electrical impedance, and ultrasonic wave propagation.

To the extent that each of these indirect methods is strongly correlated to the degree of hydration of the system, they each should provide useful measurements of the early age solidification of the cementitious system, including setting and strength development. However, each method probes a different property of the system [1]. A great opportunity is available to attempt to reconcile the results of several different methods as a way to achieve greater understanding of the complex chemical and structural changes that occur during early-age hydration.

To explore this opportunity, the Center for Advanced Cement Based Materials (ACBM) initiated a multi-laboratory study in the fall of 2004 on the early-age behavior of a single cement. Each of the previously mentioned characterization methods was used to track the course of hydration under various curing conditions. This paper reports on the results of that study and attempts to synthesize the various results in a way that might serve as a model for future investigations of this kind.

2. MATERIALS

A large quantity of proficiency sample 151 (hereafter called cement 151) was obtained from the Cement and Concrete Reference Laboratory (CCRL). This same cement was used for all the studies reported here. Proficiency sample cements are desirable for these studies because they are homogenized to ensure uniformity and they already have been subjected to a number of chemical and physical tests in about 200 independent laboratories around the world. A final report on the results of each proficiency sample is published [2]. Table 1 provides average values of selected properties of cement 151 as measured by these laboratories.

The particle size distribution of cement 151 was measured using laser diffraction through a dilute suspension of the particles in 2-isopropanol [3]. The powder was characterized by scanning electron microscopy (SEM), X-ray microprobe analysis, and quantitative X-ray diffraction (QXRD). The procedures used for these methods have been described in detail elsewhere [4,[5]]. Seven different image fields were analyzed at a magnification of 500×. Table 2 shows the mean and standard deviation for the volume fraction of each major mineral phase.

Table 1 Selected properties of CCRL cement 151 as measured by laboratories participating in the Proficiency Sample program. Measurements that were more than three standard deviations from the mean have been eliminated from the data.

Property	Average Value	Standard Deviation
Vicat Initial Setting Time	1.63 h	0.25 h
3 d Compressive Strength	27.45 MPa (3981 psi)	2.20 MPa (319 psi)
7 d Compressive Strength	33.80 MPa (4902 psi)	2.47 MPa (358 psi)
28 d Compressive Strength	41.71 MPa (6050 psi)	2.94 MPa (426 psi)
7 d Heat of Hydration	330.3 J/g	35.6 J/g
28 d Heat of Hydration	379.7 J/g	23.9 J/g

Table 2 Phase data for cement 151 powder estimated from segmented SEM images. Values are reported on a total solids basis. Uncertainty is expressed as ± one standard deviation calculated from seven images. Cement chemistry notation is used in the first four rows, e.g. C = CaO, S = SiO_2, A = Al_2O_3, and F = Fe_2O_3

Mineral	Average Volume Fraction (%)	Standard Deviation
C_3S	58.8	3.9
C_2S	17.6	3.3
C_3A	4.4	2.3
C_4AF	11.7	1.8
$CaSO_4 \cdot xH_2O$	5.6	1.0
$CaO/CaCO_3$	0.7	0.2
SiO_2	0.4	0.1
K_2SO_4	0.4	0.1
Kaolin	0.3	0.2
Periclase	0.1	0.03

3. EXPERIMENTAL METHODS

Electrical Conductivity using Impedance Spectroscopy (IS)

Electrical conductivity of a cementitious system can be measured in many ways. This study uses AC-impedance spectroscopy [6]. Two-point AC-IS measurements were made with a Solartron 1260 impedance/gain-phase analyzer [7] using Z-60 personal computer software for data acquisition. A 100 mV alternating (AC) voltage was used (1 V for the mortar cube specimens) over a frequency range of 10 MHz to 1 Hz and with twenty steps (logarithmic) per frequency decade. The impedance data were plotted in a Nyquist fashion (negative imaginary impedance versus real impedance). The real impedance value was taken at the intersection of the electrode and bulk resistance arcs.

Two specimen geometries were used in this investigation. For the studies on the time of set, a cylindrical cement paste specimen (22 mm diameter and 51 mm height) was prepared with a water-cement mass ratio (w/c) of 0.485 [8,9]. The specimen was cast inside a plastic

mold and sealed immediately to prevent moisture loss or absorption. Further, the plastic mold was submerged in a water bath to provide an isothermal curing condition at 23 ^{o}C. Additional measurements were made using 50 mm x 50 mm x 50 mm cube specimens, also with w/c = 0.485, to describe strength development. For the studies on strength development, the measurements were made using a "wet" electrode technique, in which the steel electrodes were lightly pressed against sponges soaked in a conductive ionic solution to establish intimate contact with the sample. After demolding, measurements were made in all three directions of three samples at 1 d, 3 d, and 7 d.

The electrical conductivity of the paste (σ_t) was determined by normalizing the bulk resistance for the effect of specimen and electrodes geometry:

$$\sigma_t = k/R_b \qquad \text{Eq (1)}$$

where k (in 1/m) is a geometric factor that was obtained experimentally [8] (15.76 for the set measurements and 1 for the cube measurements). Conductivity of a cement paste can be described by [10]:

$$\sigma = \sum_i \sigma_i \beta_i \phi_i \qquad \text{Eq (2)}$$

where σ_i is the conductivity, β_i the connectivity, and ϕ_i the volume fraction, of phase i (i.e., capillary porosity, hydration product, and unhydrated cement) in the hydrating cement microstructure. Since pore solution is the most conductive component in the cement paste, the equation 2 can be simplified to consider only the pore solution terms. It is believed that during set β decreases dramatically and the point of inflection on the σ_t versus time curve appears to correspond with solidification; however, further work is needed to fully test this hypothesis [9].

Time Domain Reflectometry (TDR)

Time domain reflectometry (TDR) is a form of high frequency dielectric spectroscopy that can compliment and extend the practical frequency range of other impedance/dielectric techniques, such as IS. It is a broadband technique that enables characterization over a frequency range from 10^3-10^9 Hz. The sample was arranged in a capacitance sample cell that terminates a coaxial transmission line. A signal generator sends a voltage pulse with a very short rise time (20 ps) along the transmission line. The reflected voltage pulse, which includes quantitative information about the complex dielectric properties of the sample, is detected and analyzed. A HP 54120 digitizing oscilloscope [7] with a 54121A TDR sampling head is used to generate and detect the incident and reflected transients. Consecutive segments of the TDR reflected transient are analyzed using a variable time scale sampling method [11]. The reflected transient is then transformed into the frequency domain using a numerical Laplace transform. TDR measurements were made on only one small volume of sample, with w/c = 0.485, cast into a sealed cylindrical sample cell (22 mm diameter x 37 mm length). The coaxial wire was stripped back to expose an 8 mm length of the inner conductor, which was then inserted through a Teflon disc into the fresh paste. The shield of the coaxial cable was connected by metal foil on top of the Teflon disc (but insulated from the inner conductor) to the wall of the sampling container. The Teflon disc separated the shield from the cement. TDR measurements were made every 15 min after mixing until 2 h.

Pore Solution Electrical Conductivity

Cylindrical cement paste specimens (22 mm diameter and 51 mm height) were prepared with w/c = 0.485. Pore solution was extracted from the specimens by using pressure filtration or a high pressure steel die. Pressure filtration was used for specimens in the plastic phase (0.5 h, 1 h, 2 h, and 3.5 h of age). A 0.8 μm filter was used. The pressure was provided by a high-pressure nitrogen tank and a maximum of 276 kPa (40 psi) was applied. Pore solution of the hardened specimens (5 h, 6.5 h, 8.5 h, and 10 h of age) was extracted using a high pressure steel die with a capacity of 550 MPa (80,000 psi) according to the procedure described in [12]. After extraction, pore solution was stored in small (2.5 mL) plastic containers and sealed immediately to prevent carbonation. Pore solution conductivity (σ_o) was measured using a conductivity meter connected to the impedance analyzer.

The combination of the paste conductivity and the pore solution conductivity can be used to provide information about the microstructure of the cement paste.

Ultrasonic Shear Wave Reflectometry

The principle of the wave reflection method consists of monitoring the reflection loss of ultrasonic waves with a frequency of 2.25 MHz at an interface formed by a steel plate and the cementitious material to be tested. An ultrasonic transducer is coupled to the steel plate, which, in turn, is brought in contact with the material when it is still in liquid or unhydrated state. As hydration proceeds, the wave propagation properties of the material change, which results in a variation in the reflection loss [13,14]. The minimum specimen size is approximately a 50 mm × 50 mm × 50 mm cube. Measurements are made every 10 min. The reflection loss is obtained from the amplitudes of successive reflections received from the interface between the steel plate and the material. To determine the reflection loss, the time domain of the received reflections is transformed into the frequency domain by using a fast-Fourier transform algorithm. The reflection coefficient R is then calculated from the ratio of the amplitudes of the first and second reflections received from the interface between the steel and the cementitious material [13].

When shear waves are used for the measurements and the material (e.g., cement paste) is in a liquid state, the entire wave energy, which is approaching the steel/specimen interface, is reflected, since shear waves cannot propagate in liquids. Thus, the reflection loss is zero. With continuing hydration the solids percolate and start building up a skeleton, thereby endowing the specimen with shear resistance. Shear waves therefore are able to pass the interface, with a corresponding increase in reflection loss. This time of increase previously was found to coincide with the occurrence of the percolation threshold determined by numerical simulation [15] and the onset of compressive strength measured on mortar specimens at very early ages [16]. Comparisons between time of initial set (determined by pin penetration) and time of increase in reflection loss curve showed that both values are consistently related, but are not identical [17].

The reflection loss at the interface is related to the acoustic impedance of the cementitious mixture, which is the product of density and shear wave velocity. The wave velocity is in turn a function of the shear modulus of elasticity. The shear modulus of elasticity increases with hydration. Therefore, any other property or characteristic that is related to degree of hydration should have a relationship with reflection loss. Experiments have shown that

reflection loss indeed is linearly related to direct measures of hydration, such as content of non-evaporable water, calcium hydroxide content, and chemical shrinkage [xii]. These relationships exist for approximately three days after mixing and depend on the w/c ratio of the material.

Vicat Needle for Set Time

In this study, the setting time of cement paste was measured by the Vicat Needle Test (ASTM C 101-04b). Conical ring specimens were prepared (70 mm diameter at bottom, 60 mm diameter at top, and 40 mm height) using the designated cement with w/c = 0.485. Initial and final time of set was determined using the Vicat Needle Test in accordance with ASTM C191. The time at which the Vicat needle penetrates about 25 mm into the specimen is interpreted as the initial set. The time at which the needle does not leave a complete circular impression on the paste surface is interpreted as the final set.

3.6 Deformation Measurement Using Embedded Strain Gages

The deformation of a sealed cement paste specimen was measured with a foil-type resistance strain gage embedded in a polymer composite starting from the time of casting. This method has been used in previous work to measure the autogenous and drying shrinkage of concrete [18,19]. The sensor was mounted in a 102-mm × 204-mm (4-in × 8-in) cylindrical mold using a wire suspended through the center of the mold. The holes left by the wire were then filled using a putty sealant. The sides of the mold were coated with a debonding agent to prevent friction between the mold and the specimen. Cement paste with w/c = 0.485 was mixed according to ASTM 305 in a 3.29 L (4 quart) capacity Hobart mixer. The mix water temperature was 24 °C prior to mixing and the fresh paste temperature was 23 °C immediately after casting. The mixing procedure lasted approximately 20 min, after which the cement paste was cast directly into the mold. After waiting 5 min to observe bleeding, a barrier of self-adhesive aluminum foil was applied and all joints were double sealed to prevent evaporation of moisture. No evidence of bleeding was detected during this time period. Ideally, specimens should be rotated to prevent bleeding entirely, but unfortunately the sensor wires made it impossible for this experiment. The sensor was immediately connected to a strain measurement data acquisition system with a sampling rate of 10 min. The raw strain measurement was corrected for thermal output in the fresh state using a thermal output coefficient of 13.5 μm/m/°C obtained by cycling an unrestrained strain gage through temperature steps of 20 °C and measuring total strain. Fresh cement paste does not exert stress on the strain gage, so the correction results in near zero strain output before set. At some point, the corrected reading begins to show measurable strain and a rough estimate of the set time is obtained. From that point forward the strain measurement must be re-corrected for thermal dilation. After set, the correction coefficient is 10.3 μm/m/°C, obtained from the manufacturer of the strain gage.

This measurement technique can be used to roughly estimate setting. As solidification occurs, the relative stiffness of the cement paste to the polymer embedded gage increases. At some point, the strain gage begins to register a measurable output due to autogenous shrinkage and thermal dilation. The interpretation is that the cement paste microstructure has

developed enough stiffness to transfer stress to the gage, which estimates mechanical set. For this cement paste (CCRL 151, w/c = 0.485) the estimated setting time is 5.7 h.

3.7 Chemical Shrinkage

Measurement of chemical shrinkage [20] on cement pastes was performed in this study by monitoring the change in buoyancy that occurs for samples suspended in paraffin oil. Each chemical shrinkage test consists of deaired freshly mixed cement paste that was placed in a cylindrical glass crystallization dish (80 mm diameter and 40 mm height). A 200 g sample is the typical sample size used in this study. After the cement paste was placed in the glass crystallization dish, the specimens were vibrated until a uniform amount of paste was spread over the bottom of the dish. The cement paste layer thickness was approximately 17 mm. After vibration was complete, a layer of deaired and deionized water was applied to the surface of the paste with an eyedropper until a continuous film of fluid was formed. For the normal test conditions, 10 g of water were used. It should be noted that 10 g of water was chosen for two reasons. First, it would provide sufficient fluid to compensate for the roughly 7 % volume change that may be expected during hydration. Second, it would enable the entire surface of the cement paste to be covered with water (or the ponding fluid) during the test, since slight changes in balance could provide a layer of water of varying thickness across the top of the specimen. After the addition of water to the surface of the paste, paraffin oil was applied drop by drop, until it covered the entire surface of the water in the beaker. More paraffin oil was added until the crystallization dish was nearly completely filled. The crystallization dish was positioned on a stainless steel mesh platform that was suspended with monofilament multi-purpose fishing string lines from a steel hook. The hook was connected to a string and suspended from the high-precision balance plate. The crystallization dish was then gently lowered into a plastic container filled with paraffin oil (i.e., the container included approximately 5 L of paraffin oil). To maintain a constant sample temperature, the container of paraffin oil was submerged in a temperature regulated water bath at 23 °C ± 0.2 °C with water circulation, which contained approximately 25 L of distilled water. The majority of surface of the bath was covered with an acrylic plastic lid to reduce evaporation. The balance was placed on a massive weighing table to minimize vibrations. The submerged weight of the sample was recorded automatically every 10 min from the time the specimen was placed in the bath (approximately 30 min after the addition of water to the dry cement during mixing). Chemical shrinkage measurements generally will be presented as volume change per gram of cement in the mixture (mL/g of cement).

Chemical shrinkage is the net volume change that accompanies the cement hydration reaction. Consequently, it is directly related to the extent/progress of hydration. Both the rate and extent of hydration are probed.

3.8 Autogenous Shrinkage

The measurement of autogenous strain was performed by monitoring the weight of a cement paste sample that was sealed in a membrane, submerged in paraffin oil, and suspended from a high-precision balance [20,21]. For each test, 100 to 150 g of deaired, freshly mixed cement paste was cast in a membrane. Lura and Jensen [21] have illustrated the errors that can arise if a specimen absorbs water during the test. As such, the choice was made to suspend the

specimens in paraffin oil and the membranes were carefully screened to avoid membranes that would absorb water or paraffin oil. The membranes consisted of polyurethane condoms with thickness 0.04 mm. It should be pointed out that the weight of the sample should always be monitored before and after the test to determine if liquid from the bath penetrated the membrane.

The membranes were cleaned and any lubricants were removed with a paper towel. After cleaning, the membranes were filled with cement paste. The filled membrane was tightly closed with a knot, paying careful attention to avoid the entrapment of air bubbles. The excess part of the membrane was then cut off and a monofilament line was tied to the sample. The line, approximately 400 mm long, was tied to a stainless steel hook. The sample was then gently lowered into a plastic container filled with paraffin oil that was placed in the temperature regulated water bath.

The weighing accuracy of the balance results in a nominal accuracy on the measured strain of 0.5 με, considering typical sample sizes and isotropic deformations. The actual uncertainty on the measurements is about 10 times higher, being dominated by a number of factors, including vibrations induced by the water circulation in the water bath.

3.9 Isothermal Calorimetry and Hydration Kinetics

Hydration of portland cement is an exothermic process; i.e. heat of hydration is a quantitative measure of the extent of hydration. In this study, the isothermal heat of hydration was measured on cement paste samples using an 8-channel conduction calorimeter (*TAM AIR).* Each calorimetric channel is constructed in a twin configuration, with one side for the sample and the other side for a static reference. The twin configuration enhances stability and helps canceling out noise within the system. The temperature stability of the equipment is within ± 0.02 ^{o}C, and the heat-sensing unit stability is ± 20 μ W. The samples were conditioned to the the desired temperature prior to mixing. The mixing time was around two minutes until the paste was homogeneous. The paste was charged into glass ampoules, which were then sealed to avoid moisture loss, and put into the testing channels. The average specimens weighed between 8 g and 10 g. Two specimens were tested for each mixture.

3.10 Semi-adiabatic Calorimetry

Heat development of the mortar specimen under semi-adiabatic conditions was measured for up to 14 d. This test was conducted to evaluate the proposed maturity function based on the *absolute* rate of hydration under non-isothermal conditions. The measured heat development in the concrete was converted to heat generation of paste in the concrete, based on the specific heat and mass proportions of each component. Two cylindrical specimens of 150 mm × 300 mm were tested and the average reported.

3.11 Numerical Modelling

The NIST VCCTL modeling package, which is based in part on the well known CEMHYD3D [22,23] numerical models, was used to create three-dimensional (3-D) virtual cement paste microstructures of cement 151 and to simulate their microstructure development

during hydration. The procedures for generating 3-D microstructures are reported in detail in the literature [23]. Stereological analysis was performed on the segmented SEM images described earlier, from which autocorrelation functions for each of the major clinker phases were calculated. Autocorrelation functions are used as a Gaussian filter to distribute the clinker phases statistically in three dimensions within and among the individual cement clinker particles, The particles themselves are placed with a size distribution according to that measured experimentally. The total number of particles randomly placed within a 100^3 pixel box is chosen to achieve a desired water-to-cement (w/c) ratio. Each cubic pixel in the box is 1 μm on a side.

Unflocculated cement paste microstructures with w/c = 0.485 were created and hydrated isothermally at 23 °C using VCCTL. As described elsewhere [3,4], the model performs a large number n of iterative cycles, and the simulated age of the system is estimated by a parabolic relation, $t = \beta n^2$. For cement 151, $\beta = 0.00027$ h/cycle^2 was chosen as the best overall fit to the experimental data at w/c = 0.485.

Four properties were tracked as hydration was simulated by VCCTL: degree of hydration, fraction of connected solids (an indication of initial setting time), compressive strength, and heat of hydration. Of these, the degree of hydration was used to calibrate the time conversion factor β against experimental measurements of the loss on ignition [23]of the paste hydrated to specified ages, and it will not be considered further.

4. RESULTS AND DISCUSSION

For ease of reference, the main features of each of the experimental methods described in the previous section, including estimated measurement uncertainties, have been captured in Table 3. This table illustrates the names of the methods investigated and describes the primary way in which the test method stimulates the specimen as well as how the specimen responds Table 3 discusses whether the test is well suited for laboratory or in-situ applications. It also indicates weather the test is destructive or non-destructive. Finally, information is provided as to the way that the test could be used to determine the time of solidification or the relationship with the extent of hydration that has taken place.

Table 3. Summary of early-age measurement techniques employed in ACBM multi-laboratory study

Name	Stimulus	Response	Destructive ?	In-situ/Lab	Interpretation of Set	Interpretation of DOH	Reproducibility
Electrical Conductivity using Impedance Spectroscopy	AC excitation over a frequency range (0.1 Hz to 11 MHz)	Real and imaginary impedance as a function of frequency	No	Both	Marked change in the rate of conductivity development during set	N/A	±5 % for different samples of a given mixture
Pore Solution Extraction for Chemical Composition and Electrical Conductivity	AC excitation over a frequency range (0.1 Hz to 11 MHz)	Real and imaginary impedance as a function of frequency	Yes	Lab	N/A	N/A	±5 % for different samples of a given mixture
Time Domain Reflectometry (TDR)	20 picosecond voltage pulse	Reflected voltage pulse	No	Both	Marked resistance increase at start of set	N/A	±5 % for different samples of a given mixture
Compressive Strength (ASTM C109)	Load/Stress	Displacement/Strain	Yes	Lab	Rapid gain of strength upon set	N/A	±10 % of the mean strength.
Ultrasonic Wave Reflection	High-frequency acoustic shear waves	Reflection loss	No	Both	Increase in reflection loss is related to percolation threshold	Reflection is linearly related to degree of hydration until about 3 d	±1 % for measuring amplitude of peaks

Table 3 (Continued). Summary of early-age measurement techniques employed in ACBM multi-laboratory study

Name	Stimulus	Response	Destructive ?	In-situ/Lab	Interpretation of Set	Interpretation of DOH	Reproducibility
Vicat Time of Set (ASTM C191)	Needle penetration under gravity	Resistance against penetration	Yes	Lab	25-mm penetration defined as initial set	N/A	About ±12 % for a single operator (suggested by ASTM C191)
Deformation Measurement Using Embedded Strain Gages	Passive	Strain	No	Both	Transfer of stress to gage is interpreted as mechanical set	N/A	±0.8 % error in strain gage, resolution is ± 2 με
Chemical Shrinkage	Passive	Volume of absorbed water	No	Lab	Divergence between chemical and autogenous signifies set	Volume change is proportional to degree of hydration	±5 %, based on three tests between 1 h and 24 h
Autogeneous Shrinkage (Membrane)	Passive	Volume change	No	Lab	Divergence between chemical and autogenous signifies set	N/A	±5 %, based on three tests between 1 h and 24 h
Calorimetry	Passive	Temperature, Heat	No	Lab	N/A	Measure of the heat released due to hydration	±0.02 °C in temperature, ±20 μW in power
Numerical Modeling (VCCTL)	Initial 3-D paste microstructure	Progression of microstructure development	No	N/A	Percolation threshold of solids	Mass fraction of clinker reacted	±2 % for DOH, ±30 min for set, subject to initial calibration

4.1 Time of Solidification

This section focuses on comparing the results of different testing methods with regard to the determination of solidification (setting) in the system at early ages. Figure 1 shows the relevant results of several of the methods. Most of the data in Fig. 1 were obtained from a mortar of CCRL 151 cement with w/c = 0.485 at 23 °C that was prepared in accordance with ASTM C305 using graded Ottawa sand with a sand to cement mass ratio of 2.75, with the exception of the embedded strain gage shrinkage, the isothermal calorimetry, and the VCCTL simulation (which were performed on cement paste with w/c = 0.485). For reference, the vertical dashed lines indicate the times of initial and final set as indicated by Vicat needle penetration, because this is the test with which most readers are familiar. The methods compared include the electrical conductivity of the paste, ultrasonic reflection loss, volume changed measured using an embedded strain gage, chemical and autogenous shrinkage measured volumetrically, and the volume fraction of percolated solids predicted by VCCTL simulation. Thus, the methods captured in Fig. 1 all measure different physical properties of a paste made with nominally identical materials and prepared under nominally identical conditions.

The paste conductivity test (Fig. 1a) indicates the ease with which ionic species in the pore solution can be transported through the specimen. The conductivity test is sensitive to changes in pore solution composition, pore solution volume, and pore solution connectivity (i.e., tortuosity) of the saturated pore structure. Measurements of the pore solution conductivity during the first 10 h demonstrate a slight change from 2.98 S/m at 1 h to 3.1 S/m at 2 h and 6.5 h, and 3.3 S/m at 10 h. It has been suggested [9,10] that the changes in the electrical conductivity at early ages are most directly related to changes in connectivity. As such, it has been proposed that the first derivative of conductivity with respect to time may indicate the time of set.

Figure 2 shows typical Nyquist behavior (negative imaginary impedance versus real impedance) for the electrical impedance measurements (AC-IS) and time domain reflectometry (TDR) results at 45 min. The frequency increases from right to left in the graph and corresponding numbers represent the base 10 log of frequency (Hz). The beginning of an arc seen at low frequencies (right side) is a result of the electrode behavior and is external to the specimen. At higher frequencies (left side), the bulk arc of the plain mortar is clearly evident in the TDR measurement, however this is not seen for the electrical impedance specimen. The electrical impedance specimen is unable to resolve the bulk arc of plain mortar specimens at early times (< 4 h or the time at which solidification is expected to occur) due to machine limitations. Despite this limitation in the impedance test, both measurements have a cusp between the two arcs that represents the bulk resistance (R) of the plain mortar and this cusp appears to correspond to a similar bulk resistance. It is also encouraging to note that both laboratories reporting the electrical response reported similar results even though different sample sizes and geometries were used.

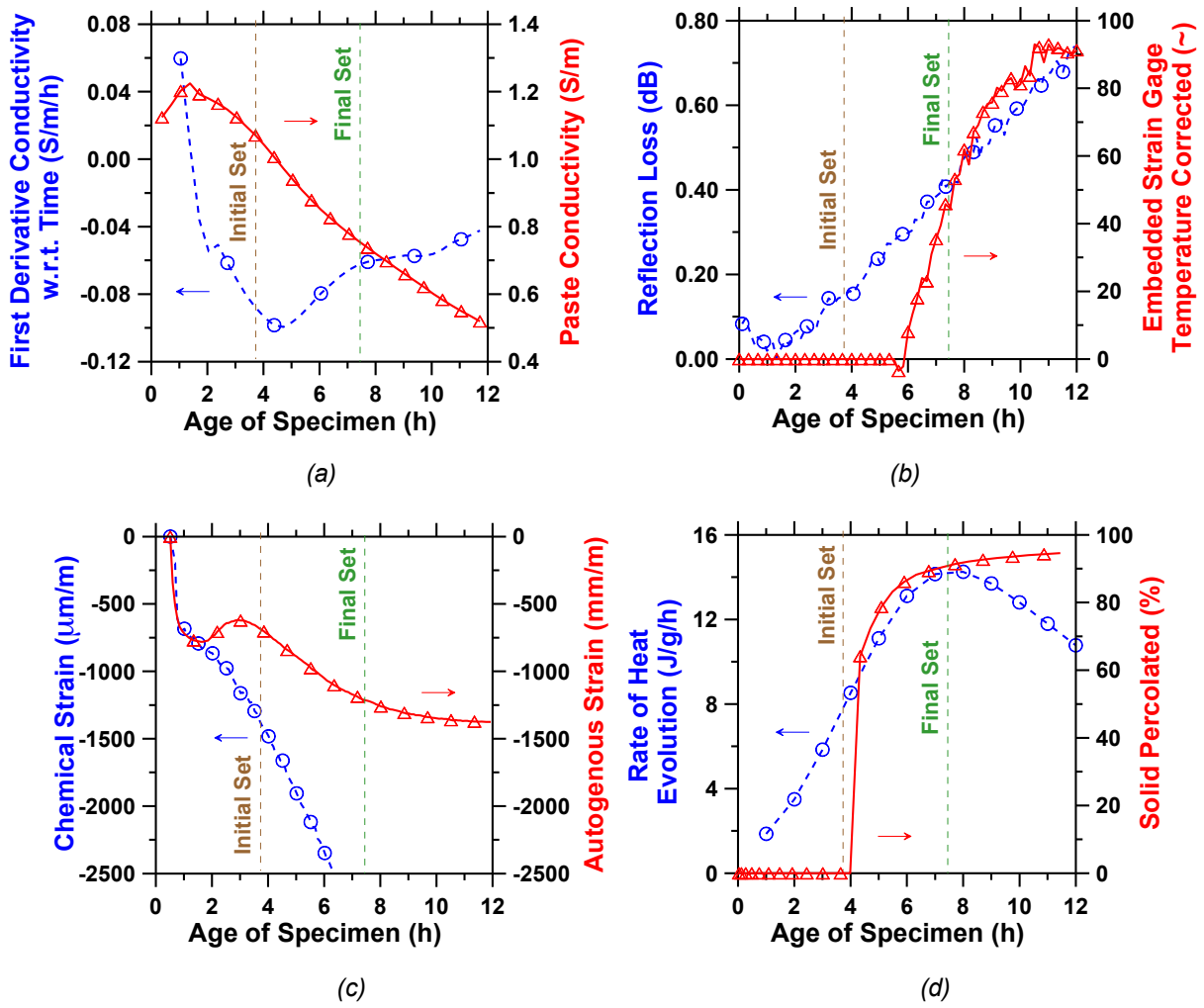

Figure 1. Comparison of results of measurements for solidification: a) cement paste conductivity and first derivative of conductivity with respect to time, b) ultrasonic reflection and embedded strain gage response, c) volumetric chemical and autogenous shrinkage, and d) isothermal calorimetry measurements at 23 °C and numerical simulation with VCCTL (solids percolation).

Figure 1b shows the results of the embedded strain gage and the ultrasonic wave reflection measurement. The ultrasonic wave reflection measurements determine the shear wave propagation properties of the material and are therefore expected to probe the developing solid structure. Shortly before the time of initial set, the reflection loss starts to increase; this behavior has been thought to be related to the increasing presence of solid microstructure [14]. The value of the reflection loss at the time of initial set is similar to previously reported results [xii]. The deformation measurement records a transfer of stress to the embedded strain gage, and therefore indicates the increasing stiffness of the bulk paste relative to the polymer gage. The principle is similar to penetration resistance methods, where external deformation is related to the relative stiffness between cement paste and the penetration apparatus. For internal deformation, the magnitude of strain reflects both the developing stiffness and the

driving forces for shrinkage and thermal dilation. Due to early creep in the cement paste specimen, the intended focus is the time of stress transfer to the gage and not necessarily the magnitudes of the strain. It should be noted that the presence of the strain gage is likely to cause the formation of an interfactial transition zone (ITZ) in the adjacent binder. An ITZ will have a higher w/c ratio than the bulk paste, and this could increase the local setting time. The magnitude of this effect has not yet been assessed.

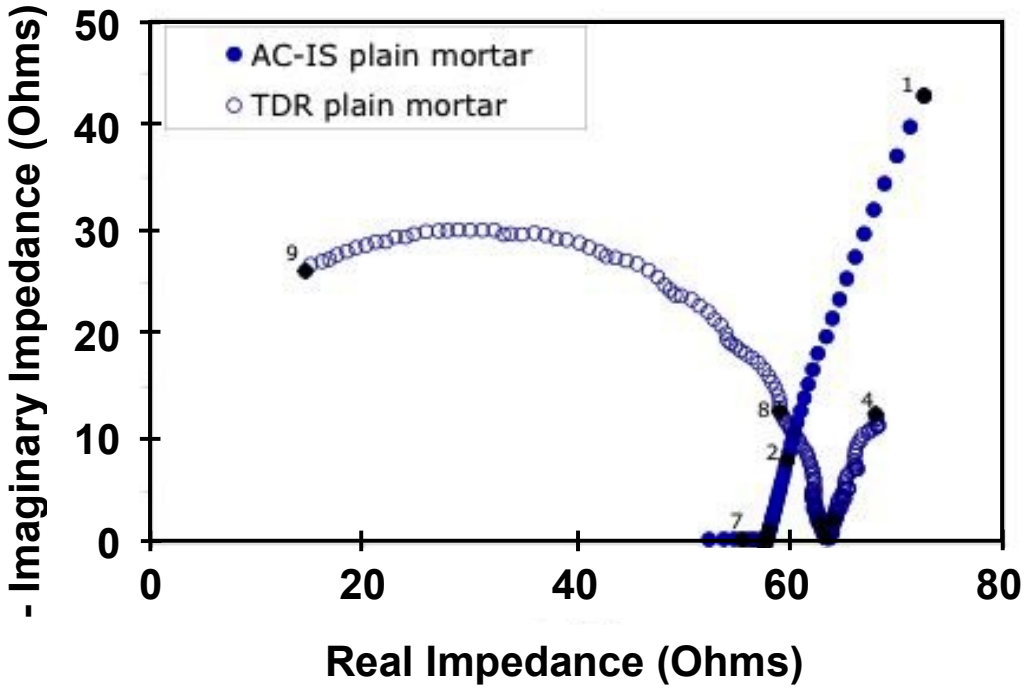

Figure 2. Nyquist plot of plain mortar measured with Electrical Impedance (AC-IS) and Time Domain Reflectrometry (TDR) at an age of 45 min.

Figure 1c shows the results of chemical and autogenous shrinkage measurements performed on a mortar specimen. Gravimetric shrinkage measurements performed on cementitious samples monitor the submerged weight change in the sample as increasing hydration results in a net reduction in volume. The chemical shrinkage measurement correlates to the degree and extent of hydration experienced by the mortar specimen while the autogenous shrinkage response describes the volumetric deformation experienced by the sample. When the mortar is in the fluid state, the chemical and autogenous responses are similar, as the fluid nature of the mortar prevents the formation of empty pores. As the mortar starts to solidify, the formation of a rigid microstructure causes the chemical and autogenous shrinkage responses to diverge as the volumetric deformation begins to stabilize and the chemical shrinkage measurement dominates. In a cement paste, the deviation in the chemical and autogenous shrinkage measurements indicates solid formation in the system. It can be seen in Fig 1c that these measurements diverge at 2 h. The appearance and subsequent re-absorption of bleed water into the sample is believed to introduce error in the experimental outcome. This would explain the swelling of the cement paste and the age discrepancy in the time of deviation (2 h) of the shrinkage response and Vicat set time of the mortar. It is

interesting to note that the end of expansion in the mortar correlates to the time of initial set (3.83 h). This may be due to the formation of a rigid skeleton at this age; however, further work is needed to investigate the effects of bleeding.

The VCCTL prediction indicates the connectedness of solids in the simulated paste, and should therefore be a direct measure of the percolation of the solid phase to the extent that the simulated microstructure is an accurate representation of the actual paste microstructure.

Correlations between the methods are immediately evident in Fig. 1. First, the peak in the heat release corresponds with the time of final set. In addtion, the VCCTL prediction of percolation correlates quite closely with the change in the rate of electrical conductivity and the initial setting time measured by the Vicat test, but seems to be uncorrelated with the Vicat final setting time. Correlations between initial set and solids percolation have been reported on other cements as well [24,25]. The observed correlation with set supports observations reported previously on other cement pastes [9]. The methods that directly probe the mechanical properties of the paste, ultrasonic reflection loss and deformation, are not correlated in any obvious way to each other. The deformation measurement is definitely sensitive to changes in the microstructure that occur during the time interval in which the other methods indicate setting to occur. This method registers transfer of stress to the strain gage about an hour after the Vicat needle penetration and the VCCTL prediction indicates initial set, although the later time indicated by the strain measurement might be attributed partly to the formation of an ITZ around the strain gage as previously noted. The increase in load resistance is similar to the sharp rise in the percolated solid fraction predicted by VCCTL, although the increase is less rapid. This is understandable if we assume that the structure formed immediately upon geometric percolation is exceptionally weak and unable to sustain loads until more solid is added to the backbone. The ultrasonic wave reflection measurement shows a steady, nearly linear, increase from an age of approximately 2 h onward. A previous report [17] has indicated that the initial increase in reflection loss (occurring at about 3 h here) is related to the time of initial set as measured by Vicat needle penetration.

4.2 Determining Strength Development

With regard to strength development, Figure 3 compares the relevant methods from among those that were used in this multi-laboratory investigation. All the experimental measurements in this case were made on mortar cubes conforming to the ASTM C109 test method for compressive strength. The VCCTL predictions were made by measuring the gel-space ratio of the simulated microstructure as a function of time, and using the relation of Powers to compute compressive strength, in which the exponent of the gel-space ratio is 2.6 and the leading coefficient is calibrated to the experimental compressive strength (ASTM C109 test method) measured at 7 d. The ultrasonic wave reflection data and electrical resistance data each have been scaled by constant conversion factors of 10 MPa/dB and 0.05 MPa/Ω, respectively, to bring them within as close agreement as possible with the ASTM C109 strength measurements. The values of heat release (Q, in J/g) have been converted to compressive strength, (σ, in MPa) using a fit determined from experimental measurements by Hansen [26]: $\sigma = 0.0001\ Q^2 + 0.0353\ Q$.

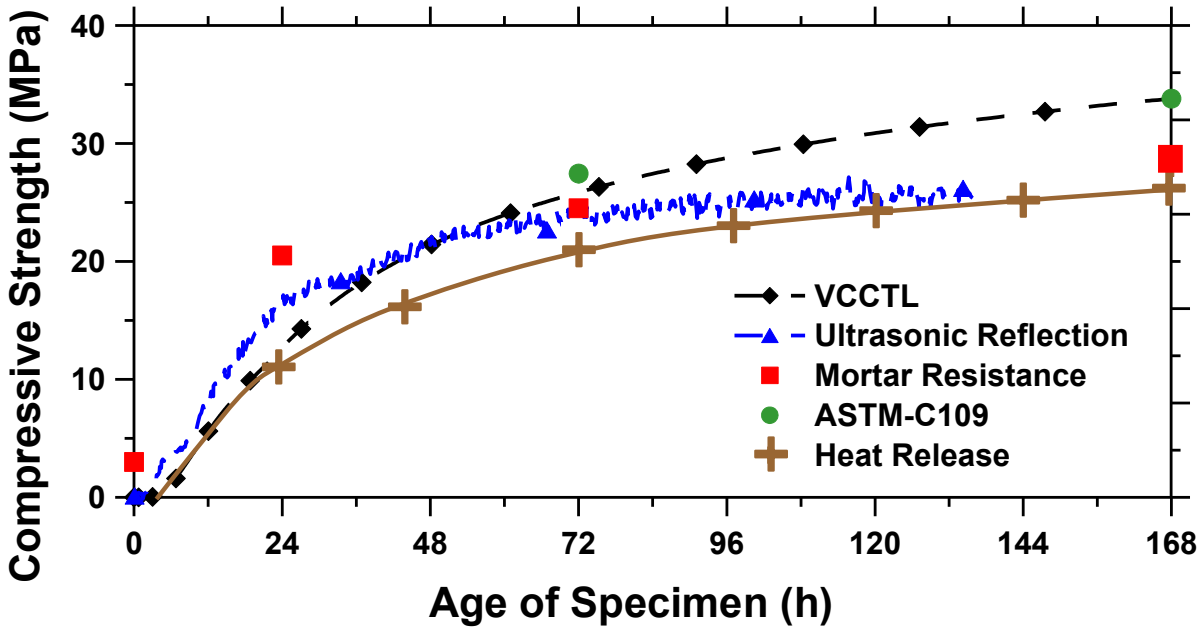

Figure 3. Comparison of measured compressive strength of mortar cubes (ASTM C109), with measurements of ultrasonic shear wave reflection loss, mortar electrical resistance, total heat release, and calculations by VCCTL model based on Powers' gel-space ratio.

Figure 3 again shows definite correlations between the methods. The VCCTL and reflection loss are in close agreement up to an age of about 48 h. At later ages, these two methods appear to diverge, with the VCCTL prediction increasing more rapidly than the reflection loss data. On the other hand, the electrical resistance of the mortar increases in a manner that is qualitatively similar to that shown by the other methods, although the increase in resistance is greater at earlier ages and lesser at later ages. An interesting trend in Fig. 5 is that the VCCTL data tend to follow the ASTM C109 measurements fairly accurately, and the ultrasonic reflection measurements tend to agree more closely with the mortar electrical resistance methods. Reasons for this apparent tracking of ultrasonic reflection and mortar electrical resistance would seem to warrant additional detailed investigation, because the agreement may be due to some common underlying structural cause. As mentioned earlier, these two methods are measuring entirely different physical quantities. Increases in electrical resistance reflect changes in the volume and tortuosity of the saturated porosity, while increases in reflection loss measures the shear modulus of the cement paste in a layer near the transducer. Neither of these is a direct measure of mortar compressive strength. The Young's modulus of concrete usually can be empirically correlated to its compressive strength [27], so one might also expect an empirical correlation between shear modulus of cement paste and the compressive strength of a mortar made from that paste. However, a true correspondence between paste shear modulus and electrical resistance of the mortar would seem to indicate a fundamental topological and morphological relation between the two interpentetrating 3-D networks in the paste itself, namely the saturated porosity and the connected solids.

Up to 7 d of hydration, the total heat release measured on concrete specimens, using cement 151 as a binder, underestimates the mortar compressive strength (see Fig. 3). However, this discrepancy should not be judged too severely for a couple reasons. First, the second-order relation used to convert heat release to compressive strength has been obtained as a best-fit relation for several different concretes using different cement binders. Second, the strength values that were used to make the correlation were obtained on *cylindrical concrete specimens* instead of ASTM C109 mortar cubes. It is somewhat surprising that the strength estimates for concrete should be lower than for mortar, but the actual strength values depend on the specimen geometry (cylindrical versus cubic) and, more importantly, on the mix proportions and the details of the mixing procedure. Slight variations in air content, for example, are known to significantly influence compressive strength.

4.3 Discussion of Temperature Effects on the Rate of Hydration

In addition to the work on setting and strength development, Hansen and co-workers at the University of Michigan have investigated methods to account for temperature effects. They have determined activation energy from heat of hydration curves (Fig 4) obtained from specimens at three temperatures 15 °C, 23 °C, and 35 ºC.

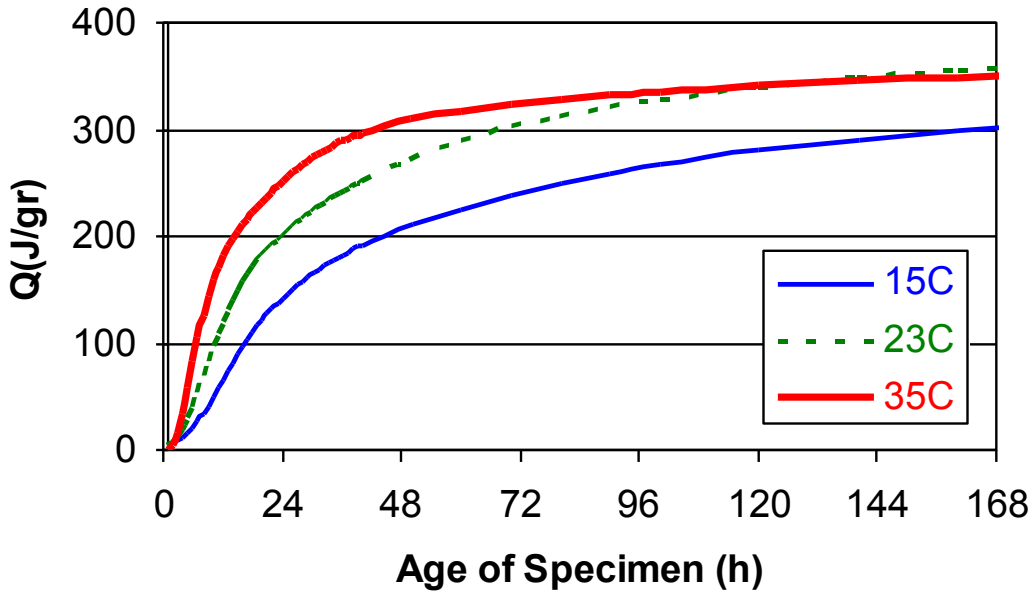

Fig 4. Cumulative heat of hydration versus time.

To obtain the activation energy, the heat of hydration curves were normalized for relative degree of hydration, here referred to as Q/Q_{100D} as shown in Figure 5, where Q is the cumulative heat of hydration, and Q_{100D} is the long-term (100 d) heat.

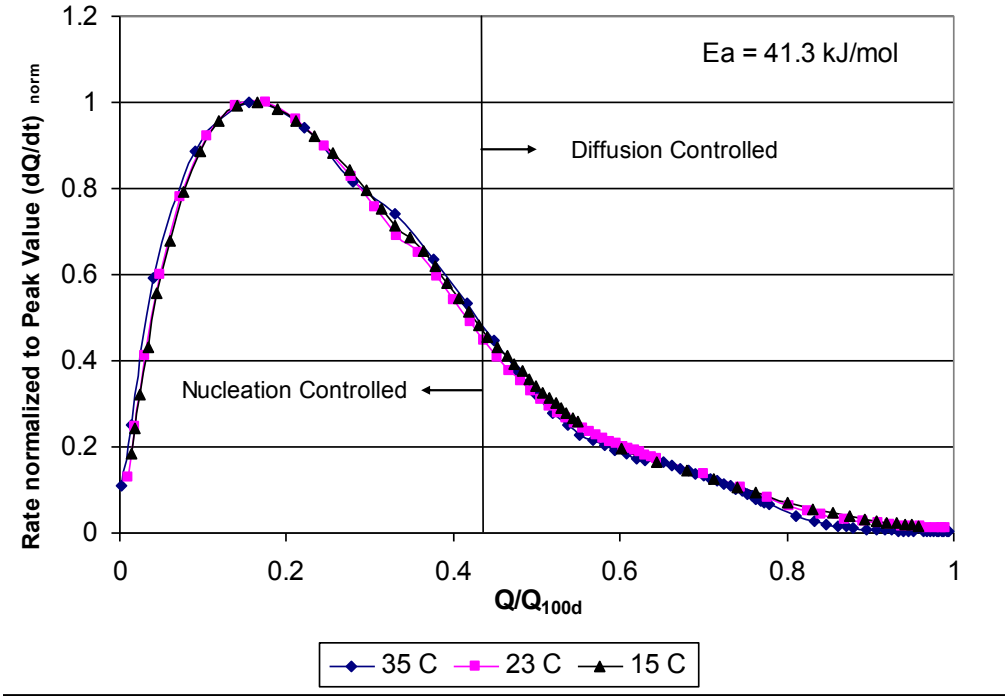

Fig 5. Changes in the rate of hydration normalized to the peak $(dQ/dt)_{norm}$ plotted versus degree of hydration (Q/Q_{100d}).

The general form of a rate function for cement hydration can be written as:

$$\frac{d\alpha}{dt} = F(T,\alpha) \qquad \text{Eq (3)}$$

where α is the degree of hydration and T is the specimen temperature. This equation is often separated into temperature-dependent and microstructure-dependent parts:

$$\frac{d\alpha}{dt} = k(T)g(\alpha) \qquad \text{Eq (4)}$$

where $g(\alpha)$ is a function of the degree of hydration and $k(T)$, the rate constant, is a function of temperature. The rate constant therefore can be calculated from:

$$k(T) = k_1 \exp[-(\frac{E_a}{RT})] \qquad \text{Eq (5)}$$

where E_a is the activation energy (J/mol) and R is the universal gas constant (8.314 J/mol/K). Using the above equations, an apparent activation energy of 41.3 kJ/mol is found from the start of hydration to about 100 d. An ongoing study by Hansen and co-workers also proposes that the total rate curves can be separated into two rate-controlling processes (i.e. nucleation followed by diffusion) as illustrated in Fig 5.

5. SUMMARY

In conclusion, this paper has reported results from a series of tests that probe different aspects of the chemical and structural properties of cementitious systems at early ages. The results

from different test methods are compared to describe the solidification. Results of the Vicat test indicate an initial set at 3.7 h and a time of final set at 7.3 h. It can be seen that the electrical conductivity tests and the ultrasonic wave reflection measurements show a change from approximately 2 h to 12 h (reduction in the case of electrical conductivity and an increase in the case of ultrasonic wave reflection). A plot of the rate of change in electrical conductivity shows a minimum at approximately 4 h. Results of the VCCTL simulation show solids percolation at approximately 4 h. The volumetric shrinkage measurements show a divergence at an age of 1.50 h, presumably due to the presence of bleed water. The embedded strain gage measurements begin at approximately 6 h. Results of the rate of strength development show a correlation with the electrical conductivity. The VCCTL data and the compressive strength also show a reasonable correlation.

REFERENCES

[1] Chapter 6.1, Weiss, W. J., "Experimental Determination of the 'Time-Zero', Early Age Cracking In Cementitious Systems". *RILEM State of the Art Report TC-EAS*. Edited by A. Bentur (2002).

[2] Final Report: Portland Cement Proficiency Samples Number 151 and 152, Cement and Concrete Reference Laboratory, 2004. www.ccrl.us/CcrlAdmin/Reports.htm.

[3] Ferraris, C., Hackley, V.A., Aviles, A.I., and Buchanan, C.E., "Analysis of the ASTM Round-Robin Test on Particle Size Distribution of Portland Cement: Phase I". *NISTIR* **6545** , U.S. Department of Commerce (2002).

[4] Bentz, D.P., Stutzman, P.E., Haecker, C.J., and Remond, S, "SEM/X-ray Imaging of Cement-Based Materials", p. 457 in *Proceedings of the 7th Euroseminar on Microscopy Applied to Building Materials* , Delft University of Technology (1999).

5 Stutzman, P. "Development of an ASTM Standard Test Method on X-Ray Powder Diffraction Analysis of Hydraulic Cements", in *Proceedings of the 52nd Annual Denver X-Ray Conference*, Steam Boat Springs, CO (2003).

[6] Woo, L. Y., Kidner, N. J., Wansom, S., and Mason, T. O., "Combined Time Domain Reflectometry and AC-Impedance Spectroscopy of Fiber-Reinforced Fresh-Cement Composites," *Cem. Concr. Res*., in press.

[7] Certain commercial instruments are identified to fully specify the experimental procedures. In no case does such identification imply endorsement by the National Institute of Standards and Technology, nor does it indicate that the instruments are necessarily the best available for the purpose.

[8] Rajabipour, F., "Fundamental Investigations on Utilizing Electrical Sensing to Improve Life-cycle Modeling of Concrete Structures", MSCE Dissertation, Purdue University, West Lafayette, Indiana (2003).

[9] Sant, G., Rajabipour, F., Fishman, P., Lura P., and Weiss, W.J., "Electrical Conductivity Measurements in Cement Paste at Early Ages", in *International Conference on Advanced Testing of Fresh Cementitious Materials*, Stuttgart, Germany (2006).

[10] Christensen, B.J., Coverdale, R.T., Olson, R.A., Ford, S.J., Garboczi, E.J., Jennings, H.M., and Mason, T.O., "Impedance Spectroscopy of Hydrating Cement-Based Materials: Measurement, Interpretation, and Application," *J. Am. Ceram. Soc.*, **77** [11], 2789-2802 (1994).

[11] Hager III, N. E., "Broadband Time-Domain-Reflectometry Dielectric Spectroscopy Using Variable-Time-Scale Sampling," *Rev. Sci. Instrum.* **65** [4] 887-891 (1994).

[12] Barneyback, R.S., "Alkali-silica Reactions in Portland Cement Concrete", Ph.D. Dissertation, Purdue University, West Lafayette, Indiana (1983).

[13] Öztürk, T., Rapoport, J.R., Popovics, J.S., and Shah, S.P., "Monitoring the Setting and Hardening of Cement-Based Materials with Ultrasound," *Concrete Science and Engineering* **1** [2] 83-91 (1999).

[14] Voigt, T., and Shah, S.P., "Properties of Early Age Portland Cement Mortar Monitored with a Shear Wave Reflection Method," *ACI Materials Journal* **101** [6] 473-482 (2004).

[15] Voigt, T., Ye, G., Sun, Z., Shah, S.P., and van Breugel, K., "Early Age Microstructure of Portland Cement Mortar Investigated by Ultrasonic Shear Waves and Numerical Simulation," *Cem. Concr. Res.*, **35** [5] 858-866 (2005).

[16] Voigt, T., Malonn, T., and Shah, S.P., "Green and Early Age Compressive Strength of Extruded Cement Mortar Monitored with Compression Tests and Ultrasonic Techniques," *Cem. Concr. Res.*, in press.

[17] Rapoport, J., Popovics, J.S., Subramaniam, K.V., and Shah, S.P., "The Use of Ultrasound to Monitor the Stiffening Process of Portland Cement Concrete with Admixtures," *ACI Materials Journal*, **97**[6] 675-683 (2000).

[18] D'Ambrosia, M.D., Lange, D. A., Grasley, Z.C., Lee, C.-J., Altoubat, S.A., and Roesler, J.R., "Instrumentation and Analysis of High Performance Concrete Bridge Decks," *J. Transportation Res. Board (TRB)* **1914** 85-96 (2005).

[19] D'Ambrosia, M.D., Lange, D.A., and Brinks, A.J., "Mechanical Performance of Self Consolidating Concrete," pp. 83-94 in *Global Construction: Ultimate Concrete Opportunities*, Dundee, Scotland (2005).

[20] Sant, G., Lura, P., and Weiss, W. J., "Measurement of Volume Change of Cementitious Materials at Early Ages: Review of Testing Protocols and Interpretation Results," *Transportation Research Record* (2006).

[21] Lura, P., and Jensen, O. M., "Measuring Techniques for Autogenous Strain of Cement Paste," in *Knud Højgaard Conference on Advanced Cement-Based Materials*, Lyngby, Denmark (2005) (also submitted to *Materials and Structures*).

[22] Bentz, D.P., "Three-Dimensional Computer Simulation of Cement Hydration and Microstructure Development," *J. Am. Ceram. Soc.* **80** [1] 3-21 (1997).

[23] Bentz, D.P., "CEMHYD3D: A Three-Dimensional Cement Hydration and Microstructural Development Modeling Package. Version 3.0". *NISTIR* **7232**, U.S. Department of Commerce (2000).

[24] Princigallo, A., Lura, P., van Breugel, K., and Levita, G., "Early Development of Properties in a Cement Paste: A Numerical and Experimental Study," *Cem. Concr. Res.* **33** [7] 1013-1020 (2003).

[25] Bentz, D.P., "Cement Hydration: Building Bridges and Dams at the Microstructure Level", in *Knud Højgaard Conference on Advanced Cement-Based Materials*, Lyngby, Denmark (2005).

[26] Hansen, W. Personal communication.

[27] Mindess, S., and Young, J.F. *Concrete*. Prentice-Hall, Englewood Cliffs, NJ (1981).